Investigation of the intrinsic properties of the electron-driven fishbone mode

A. Merle*[1], J. Decker[1], X. Garbet[1], R. Sabot[1], Z. Guimaraes-Filho[2]

[1]CEA, IRFM, F-13108 Saint-Paul-lez-Durance, France.
[2]IIFS, Université de Provence, F-13397 Marseille cedex 20, France.

1 Introduction

Populations of energetic particles generated by fusion reactions or auxiliary heating may trigger MHD modes leading to a degradation of the confinement and impact the performance of ITER-type fusion reactors. The electron-driven fishbone mode belongs to this category of plasma instabilities. They result of the interaction between the internal kink mode and energetic electrons. They have been observed in tokamaks such as DIII-D in the presence of electron heating [1] or Tore-Supra with lower hybrid current-drive [2, 3]. Since the mode resonant drive depends on the energy but not on the mass of the particles involved, the study of electron and ion fishbones are based on the same model. But as the internal kink favors the ion diamagnetic direction, the drift motion of the electrons has to be reversed for the resonant interaction to take place [4]. Using the code MIKE coupled to the relativistic Fokker-Planck code C3P0/LUKE, a recent analysis of observed electron fishbones in Tore Supra discharges emphasize the high sensitivity of the linear stability of such modes to the details of both the safety factor and the electronic distribution function. Thus electron fishbones provide a strong test for the linear stability model.

In the present work, we show how the fishbone dispersion relation [5, 4] can be modified to take into account the resonance with passing particles. The MIKE code which implements this model is introduced. It is then used for a detailed analysis of the linear stability of the electron-driven fishbone mode using a family of analytical distributions and safety factor profiles. The distributions are chosen to model those obtained in discharges heated with Electron Cyclotron Resonance Heating and with a minimum number of parameters. The influence of passing particles is then discussed.

2 Linear Dispersion Relation

The variational formalism used here for the derivation of the dispersion relation of $n = 1$ internal kink modes is the one introduced by Edery et al. in [6] and used later for the study of BAEs and GAMs by Nguyen et al. in [7]. The dispersion relation provides explicit expression for the contributions of both the fluid(thermal) part and the kinetic (fast) part of the plasma. In particular, the kinetic term is identical to the one obtained by Chen et al. [5] in the case of ions or Zonca et al. [4] in the case of electrons.

2.1 Derivation

2.1.1 The particle lagrangian

We start from the electromagnetic lagrangian,

$$\mathcal{L}(\mathbf{A},\phi) = \int \mathrm{d}^3\mathbf{x}\left(\frac{\epsilon_0\mathbf{E}^2}{2} - \frac{\mathbf{B}^2}{2\mu_0}\right) + \int \mathrm{d}^3\mathbf{x}\left(\mathbf{j}\cdot\mathbf{A} - \rho\,\phi\right), \tag{1}$$

which yields the Maxwell's equation by extremalization of the action $\int \mathrm{d}t\mathcal{L}$ against any variation of the electromatic potentials $(\mathbf{A},\phi)$. The perturbation to the system is assumed to be of the form $g =$

*antoine.merle@cea.fr

$g_\omega e^{-i\omega t}$ + c.c. (where g is any physical quantity, scalar or vector) and only the linear response of the system is considered. Then if quasineutrality is assumed, the lagrangian becomes

$$\mathcal{L}_\omega = -\int \mathrm{d}^3\mathbf{x} \frac{\mathbf{B}^*_\omega \cdot \mathbf{B}_\omega}{\mu_0} + \sum_s \mathcal{L}_{s\omega}, \tag{2}$$

with the particle lagrangian being defined for each specie as

$$\mathcal{L}_{s\omega} = \int \mathrm{d}^3\mathbf{x} \left(\mathbf{j}_{s\omega} \cdot \mathbf{A}^*_\omega - \rho_{s\omega}\, \phi^*_\omega\right). \tag{3}$$

2.1.2 A solution to the linearized Vlasov equation

All resonant effects are contained in this particle lagrangian. They can be made explicit by exhibiting a solution to the linear Vlasov equation. In doing this, one can make use of the action-angle variables derived from the unperturbed hamiltonian, which will provide an elegant form for this solution. These variables are noted $(\boldsymbol{\alpha}, \mathbf{J})$ where $\boldsymbol{\alpha}$ are the angles (α_1 is linked to the gyromotion, α_2 is linked to the poloidal motion, and α_3 to the toroidal motion) and $\mathbf{J}$ the corresponding actions (in particular, J_1 is linked to the magnetic momentum μ and J_3 to the toroidal angular momentum P_φ). The unperturbed motion has frequencies denoted by $\boldsymbol{\Omega}$ and the perturbed hamiltonian is written $h_{s\omega} = e_s\left(\phi_\omega - \mathbf{v}\cdot\mathbf{A}_\omega\right)$. All physical quantities are then expressed as the sum of Fourier modes in the angles α,

$$g_\omega = \sum_{\mathbf{n}} g_{\mathbf{n}\omega} e^{i\mathbf{n}\cdot\boldsymbol{\alpha}}, \tag{4}$$

the linearized perturbed distribution function for each specie can then be written (with F_s being the unperturbed distribution function)

$$f_{s\mathbf{n}\omega} = -\frac{\mathbf{n}\cdot\partial F_s/\partial\mathbf{J}}{\omega - \mathbf{n}\cdot\boldsymbol{\Omega}} h_{s\mathbf{n}\omega}. \tag{5}$$

2.1.3 The resonant lagrangian

One can then extract the resonances from the particle lagrangian, the process is exhibited in [6] and [7] and one obtains the resonant lagrangian

$$\mathcal{L}_{res} = \sum_{\mathbf{n}=(0,n_2,n_3)} \int \mathrm{d}^3\boldsymbol{\alpha}\, \mathrm{d}^3\mathbf{J} \frac{\omega\dfrac{\partial F_s}{\partial E} + n_3\dfrac{\partial F_s}{\partial J_3}}{\omega - \mathbf{n}\cdot\boldsymbol{\Omega}} \left|h_{s\mathbf{n}\omega}\right|^2, \tag{6}$$

where

$$h_{s\omega} = \frac{\mathbf{v}_\perp\cdot\nabla\phi_\omega}{i\omega} - v_\parallel E_{\parallel,\omega} = \frac{\mathbf{v}_{g,\perp}\cdot\nabla\phi_\omega}{i\omega}. \tag{7}$$

In deriving those expressions, one has made use of the following assumptions: the perturbation frequency is very low compared to the cyclotron frequency such that resonance with modes with $n_1 \neq 0$ is very weak, the modes are incompressible $\delta B_\parallel = 0$ and satisfy the MHD constraint $E_\parallel = 0$; all those assumptions are compatible with shear-Alfvén type modes.

2.1.4 Trapped and passing particles resonances

Even in the case of a single specie, one still has to compute the integral for every combination of mode numbers n_2 and n_3. But if the perturbation is assumed to have a single toroidal mode number and a single poloidal mode number, then only a few of those terms have a significant influence on the final result. We assume the perturbed electrostatic potential to have the following form:

$$\phi_\omega(r,\theta,\phi) = \phi_\omega(r) e^{i\mathrm{m}\theta + i\mathrm{n}\phi} \tag{8}$$

Then $(h_{s\omega})_{\mathbf{n}}$ corresponds to the following integral

$$h_{s\mathbf{n}\omega} = \frac{1}{(2\pi)^3}\int \mathrm{d}^3\boldsymbol{\alpha} \frac{\left(\mathbf{v}_g\cdot\mathbf{k}_\perp\right)\phi_\omega}{i\omega} e^{i(\mathrm{m}\theta + \mathrm{n}\phi - \mathbf{n}\cdot\boldsymbol{\alpha})}. \tag{9}$$

Before going on, the expression of the geometrical angles θ and ϕ as functions of α_2 and α_3 are reminded (see Garbet et al. [8])

$$\theta = \hat{\theta}(\alpha_2) + \delta_P\, \alpha_2, \tag{10}$$

$$\phi = \alpha_3 + q\,\hat{\theta}(\alpha_2) + \hat{\phi}(\alpha_2), \tag{11}$$

where $\hat{\theta}$ and $\hat{\phi}$ are periodic functions of α_2 and have vanishing mean value, and $\delta_P = 1$ for passing particles only. Then the frequency Ω_2 is the poloidal transit frequency ω_b and Ω_3 is the toroidal transit frequency which can be written

$$\Omega_3 = \delta_P\, q\, \omega_b + \omega_d, \tag{12}$$

where ω_d is the toroidal drift frequency, the ratio ω_d/ω_b is usually of the order of $\rho^* \ll 1$.

The integral over α_1 corresponds to a gyroaverage operator because $n_1 = 0$. One can approximate this integral by simply replacing the particle's position by the gyrocenter position.

The integral over α_3 corresponds to an integral over a great circle centered on the axis of symmetry of the torus, thus only ϕ is changing and the integral is vanishing unless $n_3 = \mathrm{n}$.

The expression for $h_{s\mathbf{n}\omega}$ then reduces to:

$$h_{s\mathbf{n}\omega} = \frac{1}{2\pi} \int \mathrm{d}\alpha_2 \frac{(\mathbf{v}_g \cdot \mathbf{k}_\perp)\, \Phi_\omega}{i\omega}\, e^{i(\mathrm{m}\theta + \mathrm{n}\phi - n\alpha_3 - n_2\alpha_2)}. \tag{13}$$

and the term in the exponential can be written (up to a factor i),

$$\mathrm{m}\left(\hat{\theta}(\alpha_2) + \delta_P\, \alpha_2\right) + \mathrm{n}\left(q\,\hat{\theta}(\alpha_2) + \hat{\phi}(\alpha_2)\right) - n_2\alpha_2. \tag{14}$$

Trapped particles For deeply trapped particles both functions $\hat{\delta}$ and $\hat{\phi}$ are negligible compared to α_2, furthermore the other term in the integral is almost independent of α_2. Then the only significant contribution to $\mathcal{L}_{res}$ will come from $\mathbf{n} = (0, 0, \mathrm{n})$ for deeply trapped particles. For weekly trapped particles, the choice of the mode number will be dictated by the resonance condition $\omega = n_2\omega_b + \mathrm{n}\omega_d$. Indeed, in this article, we will only consider modes with frequencies much lower than the typical thermal poloidal orbit frequency, so that resonance for $n_2 \neq 0$ is negligible.

Circulating particles For deeply circulating particles, the same argument as the one used for deeply trapped particles would lead us to chose $n_2 = 0$ because of the periodic motion of the particles around the magnetic axis, but if we consider the resonance condition which is in this case $\omega = (n_2 + q\,\mathrm{n})\omega_b + \mathrm{n}\omega_d$, then we need to choose n_2 such that the factor in front of ω_b is as low as possible. This can only be done by choosing $n_2 = \mathrm{m}$. Noticing that $\mathrm{m} + \mathrm{n}q \simeq k_\parallel R_0 q / B_{ax}$, the resonance with circulating particles is then restricted to the regions where $k_\parallel$ is small (around r_0).

2.2 The dispersion relation

It has been showed in [7] that all terms contained in the usual MHD energy principle [9] can be recovered from the non-resonant part of the electromagnetic lagrangian in the MHD-limit. So that if one assumes that kinetic effects are negligible as a first approximation, the potentials which minimize the action $\int \mathrm{d}t\mathcal{L}$ are similar to those obtained using the MHD energy principle.

As described in [5], the minimization is indeed a two-scale problem. If the safety factor profile is such that $q = 1$ at a radius r_0, a thin layer exists around r_0 where the gradients of the potentials are very strong and inertia plays a significant role.

Outside this layer the usual solution is recovered, and the potentials can be deduced from the radial MHD displacement $\xi_r(r) = \xi_\infty$ inside the $q = 1$ surface and 0 outside.

For the inner layer solution, the form of the solution depends on the different effects that one wishes to take into account. In all cases, the asymptotic matching between the inertial layer solution and the MHD solution yields a dispersion relation in the following form

$$\delta\hat{W}_f + \delta\hat{W}_k = \delta I, \tag{15}$$

where $\delta\hat{W}_f$ and $\delta\hat{W}_k$ are linked to the values of the non-resonant and resonant lagrangian respectively (one has $\mathcal{L} = -2\delta W$ and $\delta\hat{W} = \hat{C}\delta W$ with $\hat{C} = (\mu_0 R_0 \mathrm{m} q(r_0)^2)/(B_o^2 2\pi r_0^2 (\xi_\infty)^2)$ consistently with [4]), δI is called the inertial term and its form is dependent on the physics retained inside the inertial layer. In

this paper, we will consider the case of an inertial layer with diamagnetic effects in the limit of vanishing resistivity [10, 11] and kinetic effects of thermal ions [12], giving

$$\delta I = is\frac{\sqrt{\omega(\omega-\omega_{*i})}}{\omega_A}\sqrt{1+\left(0.5+1.6\left(R_0/r_0\right)^{1/2}\right)q^2} \equiv is\frac{\sqrt{\omega(\omega-\omega_{*i})}}{\tilde{\omega}_A} \tag{16}$$

with ω_{*i} being the ion diamagnetic frequency, ω_A the Alfvén frequency, q the safety factor and s the magnetic shear, all those quantities being evaluated at r_0 the position of the inertial layer.

2.3 Expression in gyrocenter coordinates in the limit of zero-orbit width for circular equilibria

In the case of a magnetic equilibrium with circular concentric flux-surfaces, in the limit of zero orbit width and to first order in $k_\perp\rho_s$, the jacobian of the transformation from action-angle coordinates to gyro-center coordinates $(r,\theta,\varphi,p,\xi_0,\gamma)$ (where r is the minor radius, θ and φ the poloidal and toroidal angles, p the momentum, ξ_0 the value of $p_\parallel/p$ at $\theta=0$, and γ the gyrophase) is [4]:

$$\mathcal{J}(r,\theta,\varphi,p,\xi_0,\gamma) = \frac{p^2R_0r\,|\xi_0|\,B_{ax}}{B_0(r)}\bar{\tau}_b(r,\xi_0) \tag{17}$$

where $B_0(r)=B(r,\theta=0)$ and $\bar{\tau}_b=\tau_b\cdot p/(qR_0)$ is the normalized bounce-time.

Then $\delta\hat{W}_k$ is deduced from equation (6), noting that in the limit of zero-orbit width the toroidal angular momentum $J_3\simeq -e_s\bar{\Psi}$ (with $\bar{\Psi}$ the gyro-center poloidal flux),

$$\delta\hat{W}_k = -4\pi^3\hat{C}R_0\int\frac{rB_{ax}}{B_0(r)}\mathrm{d}r\,|\xi_0|\,\bar{\tau}_b(r,\xi_0)\mathrm{d}\xi_0\,p^2\mathrm{d}p\frac{\omega\,\partial_E F_s-\frac{\mathrm{n}q}{e_srB_{ax}}\partial_rF_s}{\omega-\mathbf{n}\cdot\mathbf{\Omega}}\left|h_{s\mathrm{n}\omega}\right|^2. \tag{18}$$

3 Numerical Study

The MIKE code has been designed to compute all the terms of and solve the linear dispersion relation of the fishbone mode. It relies on the formulas derived in the previous section, equations (15),(18), (13) and (16).

The characteristics of the unperturbed particle orbits, ω_b, ω_d and $h_{s\mathbf{n}\omega}$, are calculated in the limit of zero-orbit width giving simple dependence over the particle momentum:

$$\begin{aligned}\omega_b(p,\xi_0,r) &= p\,\tilde{\omega_b}(\xi_0,r),\\ \omega_d(p,\xi_0,r) &= p^2\,\tilde{\omega_d}(\xi_0,r),\\ h_{s\mathbf{n}\omega}(p,\xi_0,r) &\simeq p^2\,\tilde{h}_{s\mathbf{n}\omega}(\xi_0,r).\end{aligned}$$

This allows us to save significant computation time, since otherwise we would have to compute these quantities for every particle momentum grid point.

For simplicity, $|h_{s\mathrm{n}\omega}|$ can be replaced by the expression obtained by integration using the ballooning transform in the case of large aspect ratio (see [5] or [4])

$$|h_{s\mathrm{n}\omega}| = \frac{e_s\mathrm{m}}{q}\,\omega_d\,\frac{\phi_\omega}{\omega} = \frac{e_s\mathrm{m}}{q}\,\omega_d\,\frac{B_{ax}r}{\mathrm{m}}\xi_\infty. \tag{19}$$

Note that this expression is exact for the case of deeply trapped particles.

The fluid term is usually calculated from the expression derived by Bussac et al. [13] for the n = 1 kink mode in toroidal geometry for the case of large aspect ratio and monotonic q-profiles,

$$\delta\hat{W}_f = 3\pi(1-q_{min})\frac{r_0^2}{R_0^2}\left(\frac{13}{144}-{\beta_{p0}}^2\right). \tag{20}$$

Also is included in the code, the contribution of fast particles to the fluid drive of the internal kink through the pressure gradient term in the usual MHD energy principle [14],

$$\delta\hat{W}_{f,h} = 4\pi^3\hat{C}R_0\int\frac{rB_{ax}}{B_0(r)}\mathrm{d}r\,|\xi_0|\,\bar{\tau}_b(r,\xi_0)\mathrm{d}\xi_0\,p^2\mathrm{d}p\,(\partial_rF_s)\,e_s\mathrm{n}\omega_d\frac{B_{ax}r}{\mathrm{m}}\,|\xi_\infty|^2 \tag{21}$$

3.1 Resonant Integral Computation

One of the first step in the computation of $\delta\hat{W}_k$ is the integral over p and it is also one of the most challenging. Because the denominator of the integrand vanishes when particles do resonate with the wave, the calculation of this integral with a classic trapezoidal approximation can lead to dramatic errors. We describe here the method used in MIKE to avoid these errors.

We first chose to treat particles going in both directions (co- and counter-current) simultaneously, that is instead of having (ξ_0, p) covering the intervals $[-1,1]\times[0,+\infty]$, they cover $[0,1]\times[-\infty,+\infty]$. The dependence of ω_b and ω_d over p implies that the denominator is a second degree polynomial and we write down the integral over p in this form

$$J(g, b_{ref}, c_{ref}) = \frac{1}{\sqrt{2}}\int_{-\infty}^{+\infty} \frac{p^4 g(p)}{p^2 + \sqrt{2}b_{ref}p - 2c_{ref}}\mathrm{d}p. \tag{22}$$

3.1.1 Integration contour

Let α_+ and α_- be the roots of the denominator,

$$\alpha_\pm = -\frac{b_{ref}}{\sqrt{2}} \pm \sqrt{\frac{b_{ref}^2}{2} + 2c_{ref}}, \tag{23}$$

because b_{ref} is real in all cases, the sum of α_+ and α_- is also real and their imaginary parts have opposite signs. α_+ is chosen to be the root with the positive imaginary part when $\mathrm{Im}\,\omega > 0$, and when $\mathrm{Im}\,\omega \leq 0$, α_+ is chosen such that its dependence over ω is analytic. The integration contour is defined to be the real axis $[-\infty,+\infty]$ when $\mathrm{Im}\,\omega > 0$, and the integral is analytically continued for $\mathrm{Im}\,\omega \leq 0$. This comes down to keeping the integration contour going below α_+ and above α_-.

3.1.2 Case of near-Maxwellian distributions

When the distribution is close to a Maxwellian distribution, then the function g decreases exponentially fast with $E = p^2/2$, and we use the plasma dispersion function Z to deal with the singular integral. It is defined as

$$Z(u) = \frac{1}{\sqrt{\pi}}\int_{-\infty}^{+\infty} \frac{e^{-u^2}\mathrm{d}u}{u - z}, \tag{24}$$

where the integration contour goes below the pole located at $u = z$.

Let the function G be defined as $G(p) = p^4 e^{p^2/2} g(p)$. We then expand the integral by decomposing the fraction in simple elements,

$$J = \frac{1}{\sqrt{2}}\frac{1}{\alpha_+ - \alpha_-}\left[\int_{-\infty}^{+\infty}\frac{G(p)-G(\alpha_+)}{p-\alpha_+}e^{-p^2/2}\mathrm{d}p - \int_{-\infty}^{+\infty}\frac{G(p)-G(\alpha_-)}{p-\alpha_-}e^{-p^2/2}\mathrm{d}p + \ldots \right.$$
$$\left. G(\alpha_+)\int_{-\infty}^{+\infty}\frac{e^{-p^2/2}\mathrm{d}p}{p-\alpha_+} - G(\alpha_-)\int_{-\infty}^{+\infty}\frac{e^{-p^2/2}\mathrm{d}p}{p-\alpha_-}\right] \tag{25}$$

The two last integrals contain all the singularities, and J can be expressed as,

$$J = \frac{1}{\sqrt{2}}\frac{1}{\alpha_+ - \alpha_-}\left[\int_{-\infty}^{+\infty}\frac{G(p)-G(\alpha_+)}{p-\alpha_+}e^{-p^2/2}\mathrm{d}p - \int_{-\infty}^{+\infty}\frac{G(p)-G(\alpha_-)}{p-\alpha_-}e^{-p^2/2}\mathrm{d}p + \ldots \right.$$
$$\left. \sqrt{\pi}G(\alpha_+)Z\left(\frac{\alpha_+}{\sqrt{2}}\right) - \sqrt{\pi}G(\alpha_-)\left(-Z\left(-\frac{\alpha_-}{\sqrt{2}}\right)\right)\right]. \tag{26}$$

The first two integrals are regular and can be dealt with by using a trapezoidal approximation.

This method is most effective when used with near-Maxwellian distributions, should this not be the case, one could use the same method without the exponential factor in the definition of g such that the plasma dispersion function would be replaced by a logarithm.

3.2 Solving the dispersion relation

The code MIKE solves the linear dispersion relation for fishbone-like modes using a method first described by Davies [15].

This method is based on the residue theorem to compute the zeros of an analytic function. The details of the method can be found in the original article by Davies [15]. We recall here some of the key features of this method.

The problem, as initially formulated by Davies is to find the zeros of a given complex function $z \to h(z)$ inside the unit circle ($|z| < 1$). The first step is to compute the number of zeros inside the unit circle. For this we evaluate h on N equally spaced points along this circle, and we increase N until the change in modulus and argument between two successive values of h is sufficiently small. The overall change of argument of h along the circle is equal to the number of zeros times 2π. The next and final step is the computation of some integrals (using those N points) that are symmetric functions of the zeros.

We would like to point out two things.

- The number N influences the precision of the computation of the integrals and thus the precision in the computation of the zeros, so that choosing more restrictive conditions for the change in modulus and argument will improve the accuracy of the method.
- Because the method is applicable to any analytical function, we can compose h with any conformal map of the complex plane, effectively changing the shape of the circle to any regular contour. This can be used to look for zeros inside circles with radii bigger, or smaller, than 1 and centered at any point in the complex plane, but also to use shapes that are more complex, like an ellipse.

4 Intrinsic Properties

In this section, we use the MIKE code to study the stability of the n = 1 internal kink mode in the presence of fast electrons using analytical distribution functions of fast electrons that mimic those obtained in ECRH-experiments. As a first approximation we will only include the resonant effects of trapped particles in $\delta\hat{W}_k$, the effect of the addition of circulating particles is discussed later.

4.1 Choice of parameters

4.1.1 Equilibrium

The equilibrium is chosen to be low-beta, high aspect ratio with circular concentric flux surfaces. To describe the equilibrium, we need to specify the aspect ratio and the safety factor. For the aspect ratio, the value of $R_0/a = 3$ is retained as a typical value for present-day tokamaks (except for spherical tokamaks).

The safety factor profile will be assumed to be parabolic with a null derivative at the origin. The position of the $q = 1$ surface is fixed at $r_0 = a/5$ (also quite typical for electron-fishbone experiments) and the magnetic shear at $q = 1$, s is left as a free parameter. Then q is written

$$q(r) = \frac{s}{2}\left(\left(\frac{r}{r_0}\right)^2 - 1\right) + 1. \tag{27}$$

And we have for the value of q on axis

$$q_0 = 1 - \frac{s}{2}. \tag{28}$$

4.1.2 Distribution function

To model the case of ECRH-heated plasmas, the electronic distribution function is chosen to have a Maxwellian form with an anisotropic temperature,

$$f(p, \xi_0, r) = \tilde{f}(r) \exp\left(-\frac{p^2}{2m_e k_B T(\xi_0)}\right). \tag{29}$$

For the function $T(\xi_0)$, we consider a modification of the 2-temperatures model where $1/T(\xi_0) = {\xi_0}^2/T_\parallel + (1 - {\xi_0}^2)/T_\perp$. Now the model contains a third temperature $T_t = T(\xi_{0,T})$ where $\xi_{0,T}$ is the position of the

trapped-passing boundary at the $q = 1$ surface. The polynomial dependence of $1/T$ on ξ_0^2 is conserved and we suppose that the temperature is maximal at $\xi_{0,T}$. We obtain

$$\frac{1}{T(\xi_0)} = \left[\left(\left(\frac{1}{T_\parallel} - \frac{1}{T_t}\right)\frac{\xi_{0,T}^4}{(1-\xi_{0,T}^2)^2} - \left(\frac{1}{T_\perp} - \frac{1}{T_t}\right)\right)\xi_0^2 + \left(\frac{1}{T_\perp} - \frac{1}{T_t}\right)\right]\left(\frac{\xi_0^2}{\xi_{0,T}^2} - 1\right)^2 + \frac{1}{T_t}. \tag{30}$$

To further reduce the number of parameters, we make the assumption that the 3 temperatures are linked, and we relate $T_\perp$ to T_t and $T_\parallel$ by the relation

$$T_\perp = T_\parallel + (T_t - T_\parallel)(1 - 2\xi_{0,T}^2). \tag{31}$$

In this way, when $\xi_{0,T} = 0$, $T_\perp = T_t$ and when $\xi_{0,T}^2 = 1/2$, $T_\perp = T_\parallel$.

The local flux-surface averaged volume element is (see [16]),

$$\mathrm{d}V(r) = 4\pi^2 \left(\frac{1}{2\pi}\int_0^{2\pi} \frac{B_{ax}}{B^\theta}\mathrm{d}\theta\right)\cdot\left(\frac{1}{2\pi}\int_0^{2\pi}\frac{B}{B^\theta}\mathrm{d}\theta\right)^{-1}\mathrm{d}r = 4\pi^2\sqrt{\frac{1-\epsilon}{1+\epsilon}} \tag{32}$$

with $\epsilon = r/R_0$, so that the flux-surface averaged electronic density is

$$n(r) = 2\pi\sqrt{\frac{1+\epsilon}{1-\epsilon}}\tilde{f}(r)\int_{-1}^{1}|\xi_0|\,\bar{\tau}_b(r,\xi_0)\,\mathrm{d}\xi_0\int_{-\infty}^{+\infty}p^2\,\mathrm{d}p\exp\left(-\frac{p^2}{2m_e k_B T(\xi_0)}\right) \tag{33}$$

We see that the $\tilde{f}$ function is closely related to the density of particles. A reasonable first approximation for n is to take a linear function between 0 and r_0,

$$n(r) = n_h\,\frac{r}{r_0}, \tag{34}$$

where n_h is a constant and one has

$$\tilde{f}(r) = \frac{n_h\, r/r_0}{\tilde{I}(r)}, \tag{35}$$

where

$$\tilde{I}(r) = \frac{1}{2}\sqrt{\frac{1+\epsilon}{1-\epsilon}}\int_{-1}^{1}|\xi_0|\,\bar{\tau}_b(r,\xi_0)\,\mathrm{d}\xi_0\,(2\pi m_e k_B T(\xi_0))^{3/2}. \tag{36}$$

4.1.3 Summary

The equilibrium is described using a single parameter, the magnetic shear at the $q = 1$ surface. The distribution function is described by only two parameters, the density at $q = 1$, noted n_h and the ratio $T_t/T_\parallel$. An example of the obtained distribution function is displayed in figure 1.

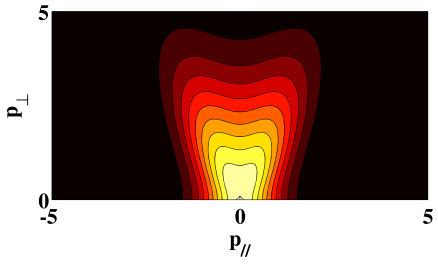

Figure 1: Contours of the distribution function in $(p_\parallel, p_\perp)$ space for $T_t/T_\parallel = 10.1$.

4.1.4 Additional assumptions

High frequency modes We will only consider modes that have a frequency much higher than the ion diamagnetic frequency ω_{*i} such that it will have a very weak influence on the solution of the dispersion relation. Thus we set $\omega_{*i} = 0$, but as we will only be looking for modes rotating in the ion diamagnetic direction ($\mathrm{Re}\,\omega > 0$) the influence of ω_{*i} is not completely lost.

Marginal stability We impose $\mathrm{Im}\,\omega = 0$, such that modes are at marginal stability. This will provide us a clear view of the stability condition as well as a simple interpretation of the imaginary part of $\delta\hat{W}_k$. Indeed, only resonant particles ($\omega = \mathrm{m}\delta_P\omega_b + \mathrm{n}\omega_d$) will contribute to $\mathrm{Im}\,\delta\hat{W}_k$ and the sign of the contribution is mainly linked to the radial gradient of the distribution function at the position of the resonance.

4.1.5 Numerical Procedure

With these two additional assumptions, we adopt the following procedure.

We have 5 real variables or unfixed parameters: s, $T_t/T_\parallel$, n_h, ω and $\delta\hat{W}_f$ (or equivalently β_p). Solving the dispersion relation will allow us to express 2 of those as functions of the 3 others; we choose s, $T_t/T_\parallel$ and ω as the variables. For each value of s and $T_t/T_\parallel$, and fixing $n_h = 1$, we compute $\delta\hat{W}_k$ for a wide range of values of $\mathrm{Re}\,\omega$. Separating the real and imaginary parts of the dispersion relation, we obtain the following solution for n_h and $\delta\hat{W}_f$:

$$n_h(s, T_t/T_\parallel, \omega) = \frac{s|\omega|/\tilde{\omega}_A}{\mathrm{Im}\,\delta\hat{W}_k(\omega)\Big|_{n_h=1}}, \tag{37}$$

$$\delta\hat{W}_f(s, T_t/T_\parallel, \omega) = \frac{s|\omega|/\tilde{\omega}_A}{\mathrm{Im}\,\delta\hat{W}_k(\omega)\Big|_{n_h=1}} \cdot \left(\mathrm{Re}\,\delta\hat{W}_k(\omega) + \delta\hat{W}_{f,h}\right)_{n_h=1}. \tag{38}$$

Instead of $\delta\hat{W}_f$, we will use the ideal growth rate of the kink mode namely

$$\gamma_I = -\frac{\tilde{\omega}_A}{s}\delta\hat{W}_f. \tag{39}$$

4.2 Results

4.2.1 Effect of $\delta\hat{W}_f$

We applied this procedure for standard values, $s = 0.05$, $T_t/T_\parallel = 10.1$ and ω ranging from 0 to about $26\,kHz$ (additional relevant physical parameters were $R_0 = 3\,m$, $a_p = 1\,m$, $B_{ax} = 4\,T$, $k_B T_\parallel = 10\,keV$).

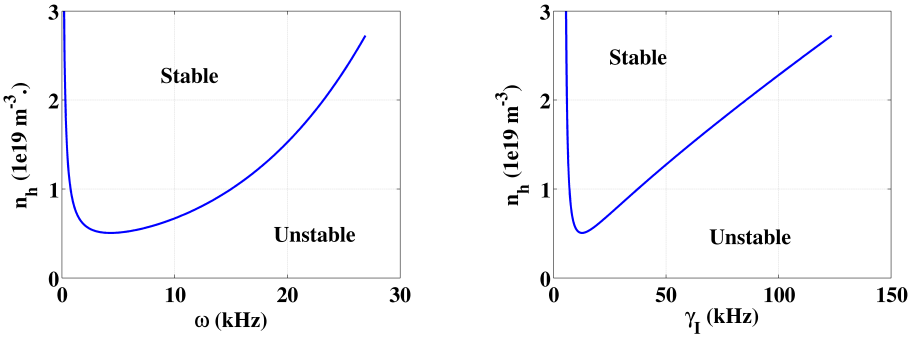

(a) $n_h(\omega)$. (b) $n_h(\gamma_I)$.

Figure 2: $n_h(\omega)$ and $n_h(\gamma_I)$ for $s = 0.05$ and $T_t/T_\parallel = 10.1$ with trapped particles only.

The results for n_h are presented in figure 2 . One striking feature is that it reaches a minimum for a given frequency (or fluid drive).

This is the result of the interplay between the energy of the resonant electrons and the level of F at this energy. As ω goes to 0, the energy of the resonant electrons goes to 0 as well and thus $(\mathrm{Im}\,\delta\hat{W}_k)|_{n_h=1}$ goes to 0 faster than ω, so that n_h goes to infinity. For high frequencies, there are not enough resonant electrons for them to have a significant contribution to $(\mathrm{Im}\,\delta\hat{W}_k)$ which will go to 0 as ω goes to infinity, so that n_h will go to infinity. In between these two extrema n_h must reach a minimum.

Figure 2b tells us that the solutions found all correspond to the stabilization of an ideally unstable mode in the absence of fast particles ($\gamma_I > 0$). It seems that although there is a net transfer of energy to the wave ($\mathrm{Re}\,\omega \cdot \mathrm{Im}\,\delta\hat{W}_k > 0$), this is still not enough to drive an ideally stable mode.

The frequency of the minimum ω_0 is the frequency where the linear drive by the resonant trapped electrons is the most effective. For this set of parameters, the value at the minimum n_{h0} is a critical value beow which the ideally unstable internal kink cannot be stabilized.

4.2.2 Effect of s and $T_t/T_\parallel$

We then varied s and $T_t/T_\parallel$ around those values to study the effect of each of these parameters on n_{h0}. As can be seen in figure 3a, n_{h0} is mostly influenced by s.

In the region of low magnetic shear ($s < 0.1$), n_{h0} is almost proportional to s. In this region, the q-profile is almost flat and the amount of electrons with a reversed drift frequency is almost constant such that $\delta\hat{W}_k$ is almost independent of s and equation (37) gives the proportionality between n_{h0} and s.

At higher magnetic shear, the population of electrons with a reversed drift frequency will decrease as we increase the magnetic shear. As a consequence, $\delta\hat{W}_k$ will also decrease and n_{h0} will grow faster than s.

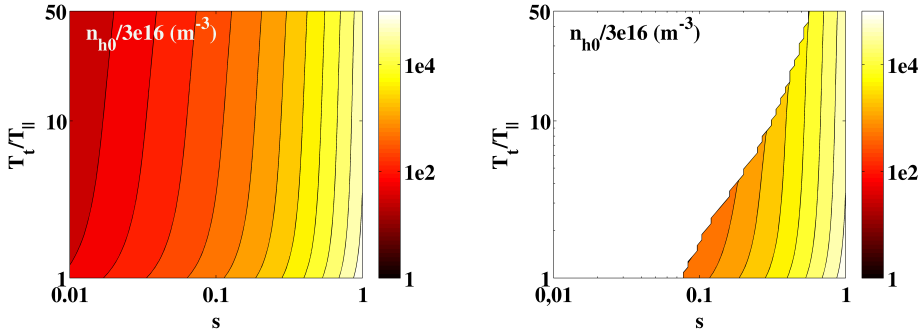

(a) Trapped particles only. (b) With passing particles.

Figure 3: Isocontours of n_{h0} against s and $T_t/T_\parallel$.

4.3 Effect of passing particles

The same simulations were then ran enabling the resonant interaction between the mode and the passing particles.

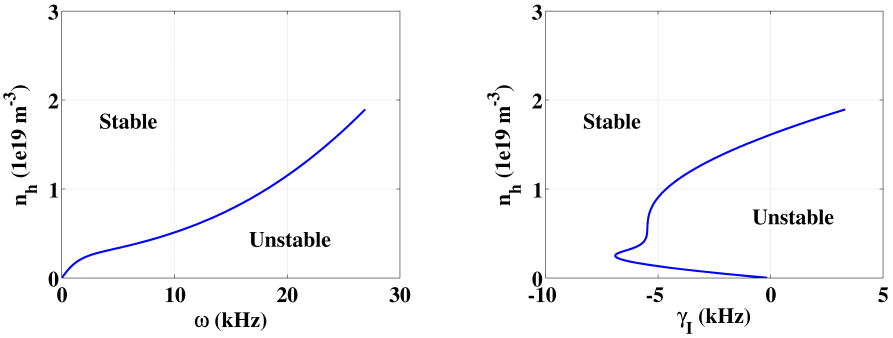

(a) $n_h(\omega)$. (b) $n_h(\gamma_I)$.

Figure 4: $n_h(\omega)$ and $n_h(\gamma_I)$ for $s = 0.05$ and $T_t/T_\parallel = 10.1$ including passing particles.

4.3.1 Resonance at low frequency

Comparing, figure 4a with figure 2a, we notice that n_h does not go to infinity as ω goes to 0 when passing particles are added. The reason being that the behavior of $\delta\hat{W}_k$ at low frequency is completely changed by the addition of passing particles resonance.

Consider for example $\omega = 0$, the resonance condition becomes $(q-1)\omega_b = \omega_d$. Because ω_d/ω_b for thermal electrons is of the order of ρ^*, if $q-1$ is of the order of unity then the resonance condition can only be met for very energetic electrons. But if s is small then $q-1$ will be small everywhere inside the $q=1$ surface and there will be enough resonant particles for their contribution to $(\mathrm{Im}\,\delta\hat{W}_k)$ to be non-negligible.

If $\omega > 0$ but remains small compared to the bounce-frequency of thermal electrons, then the same argument can be used and the contribution of passing particles to $(\mathrm{Im}\,\delta\hat{W}_k)$ will be of the same order as for $\omega = 0$. Figure 5 shows $(\mathrm{Im}\,\delta\hat{W}_k)$ against ω with or without passing particles resonance, the difference between the two curves appears to be almost constant across the range of ω.

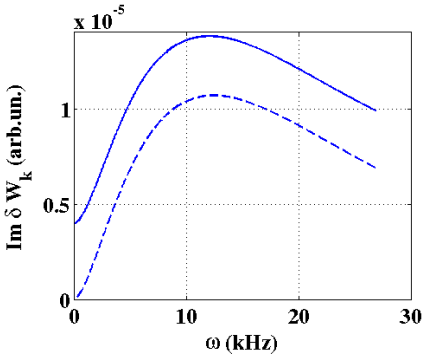

Figure 5: $\mathrm{Im}\,\delta\hat{W}_k(\omega)$ for $s = 0.05$ and $T_t/T_\parallel = 10.1$ with (solid) and without (dashed) passing particles resonance.

4.3.2 Destabilization of an ideally stable mode

Looking at figure 4b, it appears that the addition of passing particles enables the destabilization of an ideally stable internal kink with a finite fast electrons density. This branch is then stabilized again at higher frequency. This is most probably due to the fact that the energy exchange between particles and mode is greater in this case.

4.3.3 Influence of magnetic shear

As pointed out in section 4.3.1, a weak magnetic shear is needed for the passing particles to significantly influence the value of $\delta\hat{W}_k$. But if s is strong enough for $(\mathrm{Im}\,\delta\hat{W}_k)$ to be small at $\omega = 0$, then n_h will be close to its value with trapped particles only except for ω close to 0, and a (local) minimum for n_h can be recovered. On figure 3b, we observe that for $s > 0.1$, this minimum is indeed recovered and its value is close to the one with trapped particles only.

5 Summary

The original fishbone dispersion relation has been extended to account for resonance with passing particles in the limit of zero-orbit width. The MIKE code has been developed to solve this dispersion relation for the case of the internal kink mode. It has been used to study the stability of electron-driven fishbone modes using analytical distribution functions of electrons modeling those obtained experimentally with ECRH. Results from those simulations, in agreement with analytical theory, show that low-shear safety factor profiles enhance the influence of fast electrons on the internal kink mode. For the class of distributions considered, only the inclusion of resonant effects of passing electrons allows the destabilization of ideally stable modes.

References

[1] K. Wong et al. *Physical Review Letters*, **85**(5), 996 (2000).

[2] M. Goniche et al. *Fusion Science and Technology*, **53**(1), 88 (2008).

[3] A. Macor et al. *Phys. Rev. Lett.*, **102**(15) (2009).

[4] F. Zonca et al. *Nuclear Fusion*, **47**, 1588 (2007).

[5] L. Chen et al. *Phys. Rev. Lett.*, **52**(13), 1122 (1984).

[6] D. Edery et al. *Plasma Physics and Controlled Fusion*, **34**(6), 1089 (1992).

[7] C. Nguyen et al. *Physics of Plasmas*, **15**(11), 112502 (2008).

[8] J. Garcia et al. *Nucl. Fusion*, **50**(2) (2010).

[9] I. B. Bernstein et al. *Proc. of the Royal Society of London.*, **244**(1236), 17 (1958).

[10] B. Coppi et al. *Nuclear Fusion*, **6**(2), 101 (1966).

[11] G. Ara et al. *Annals of Physics*, **112**(2), 443 (1978).

[12] J. P. Graves et al. *Plasma Physics and Controlled Fusion*, **42**(10), 1049 (2000).

[13] M. N. Bussac et al. *Phys. Rev. Lett.*, **35**(24), 1638 (1975).

[14] R. B. White et al. **28**(1), 278 (1985).

[15] B. Davies. *J. Comput. Phys.*, **66**(1), 36 (1986).

[16] J. Decker et al. *Submitted to Comp. Phys. Comm.* (2008).